SEMARAK ILMU PUBLISHING

Journal of Advanced Research in Applied Sciences and Engineering Technology

Journal homepage:
https://semarakilmu.com.my/journals/index.php/applied_sciences_eng_tech/index
ISSN: 2462-1943

Chattering Analysis of an Optimized Model Free Sliding Mode Controller for a DC Motor Speed Control

Edvin Priatna[1,2,*], Rukmi Sari Hartati[1], Ida Bagus Gede Manuaba[1], I Made Oka Widyantara [1], Nurul Hiron[2].

[1] Department of Electrical Engineering, Udayana University, Indonesia
[2] Department of Electrical Engineering, Siliwangi University, Indonesia

ARTICLE INFO

Article history:
Received 2 March 2024
Received in revised form 13 July 2024
Accepted 15 August 2024
Available online 2 September 2024

Keywords:
Chattering; Control; Switching function; Dc motor; Optimization

ABSTRACT

The purpose of this study is to examine the chattering phenomenon in DC motor speed control technique using Model Free Sliding Mode Controller (MFSMC). The method used is to manipulate the switching tnah function and switching sign function in the Grey Wolf Optimizer (GWO) model and Velocity Aided Grey Wolf Optimizer (VAGWO) algorithm. The model is analyzed by MATLAB and SIMULINK programs through control model and DC motor model. The study results show that chattering of DC motor speed control is greatly eliminated by using the hyperbolic tangent function (tanh) instead of the signum function. Therefore, it can be concluded that the performance of MFSMC can be greatly improved by manipulating the switching function. The tanh switching function in motor speed control can affect Gradual Change so as to reduce the possibility of sudden or drastic changes in control output that can cause chattering, besides the tangent switching function can help reduce system sensitivity to disturbances or noise. The use of MFSMCs with hyperbolic switching functions can lead to an increase in the lifetime of electric motors, and improve the reliability of power quality in grid systems.

1. Introduction

Chattering, an undesirable phenomenon characterized by high-frequency oscillations in the control signal, is a significant challenge in sliding mode control (SMC) systems. To reduce chattering in Model Free Sliding Mode Controller (MFSMC) implemented with optimization algorithms such as Grey Wolf Optimizer (GWO) and Velocity Aided Grey Wolf Optimizer (VAGWO). The study delves into chattering in DC motor speed control via the Model Free Sliding Mode Controller (MFSMC), comparing the efficacy of hyperbolic tangent (tanh) and signum (sign) switching functions within the Grey Wolf Optimizer (GWO) and Velocity Aided Grey Wolf Optimizer (VAGWO) models.

The switching sign function is responsible for determining the direction of the control input, while the tanh function helps in controlling the rate of change of the control signal. In the context of

* *Corresponding author.*
E-mail address: edvinpriatna@unsil.ac.id

https://doi.org/10.37934/araset.51.1.229244

chattering elimination, the switching sign function dictates the polarity of the control input, ensuring smoother transitions and reducing abrupt changes. On the other hand, the tanh function aids in controlling the rate of change, effectively smoothing out rapid fluctuations and contributing to improved stability in the system.

Utilizing MATLAB and SIMULINK, the research aims to mitigate chattering, a prevalent issue in sliding mode control systems, by investigating which switching function offers smoother control signal transitions. This analysis holds implications for optimizing control strategies in engineering applications, particularly DC motor speed control, to enhance system stability and reliability.

In this research paper, we present an innovative approach to the speed control of a DC motor using an optimized model-free sliding mode controller (SMC). The primary objective of this study is to address the challenges associated with chattering, a common issue that arises in conventional sliding mode control (SMC) techniques, by introducing modifications to the sign function and the tanh function within the controller design. The DC motor is utilized as the plant in this study, and its parameters are as follows: Armature resistance (Ra) was 0.4 Ohm, Armature inductance (L_a) was 2.7 Henry, Moment of inertia (J) was 0.0004 kg.m^2, Viscous friction of 0.0022 N.m.s/rad, Torque coefficient (K_t) was 0.015 N.m/A, and Back emf coefficient (K_b) was 0.05 V.s. The novelty of this work lies in three key aspects: the use of a DC motor as the plant, the modification of the sign function and tanh function within the GWAO and VAGWO algorithms, and the detailed analysis of the chattering

The system model in conventional sliding mode control [1], is incorporated into the control law by substituting the model for the derivative of the highest order state into the expression for the time derivative of the sliding surface, which must be equal to zero once on the surface. Chattering problem often occurs in sliding mode design [2], to reduce the chattering effect is used a boundary layer in the control law form. Tracking precision was reduced but the control effort became smooth, which is required in most of control system applications. The model free SMC approach is based on previous control inputs, state measurements and the knowledge of the system order, the derivation process follows the format of conventional SMC but with the system model replaced with the approximation [3-5]. Some results on proportional integral derivative and model free sliding mode control are sliding mode control on multi input multi output system [6], control of twin rotor aerodynamic systems [7], comparing of PID and sliding mode controllers for quadrotor [8], controller of reverse osmosis desalination plants [9], load frequency control in microgrid with electrical vehicle [10], control of [8], control of unmanned aircraft system [5], speed regulation of permanent magnet synchronous motor [11], balance control of vehicle system [12], regulate blood glucose level [13], robotic exoskeleton [14], soft landing control of single-coil reluctance actuators [15], speed control of DC motor [16]. The chattering phenomenon in industrial control systems refers to the rapid and erratic switching of the control signal [17], which can lead to undesirable vibrations and wear in mechanical components. The chattering phenomenon in the controller system can have a significant impact on the speed of the DC motor [18]. The rapid and erratic switching of the control signal can lead to rapid fluctuations in the motor speed, causing instability and oscillations in the system [19]. This can result in increased wear and tear on mechanical components, decreased precision in speed control, and reduced overall system performance.

The Grey Wolf Optimizer and Velocity Aided Grey Wolf Optimizer are effective tools for chattering elimination in industrial control systems [20]. Research has shown that by manipulating the switching tanh function and switching sign function within these optimization models, the chattering phenomenon can be significantly mitigated. These functions play a crucial role in controlling the rapid and erratic switching of the control signal, thereby reducing undesirable vibrations and wear in mechanical components.

The switching sign function is responsible for determining the direction of the control input, while the tanh function helps in controlling the rate of change of the control signal. By optimizing these functions within the GWO and VAGWO models, the abrupt changes in the control input due to chattering can be smoothed out, leading to improved stability and reduced oscillations in the system [21].

This study analyses the vibration that occurs in DC motor speed control using a model-less optimised sliding mode controller. Previous studies by Firdaus et al [22] demonstrated the importance of DC motor speed control systems with PID controllers, which provided a foundation for further research in the development of more advanced control techniques. Azeem and Zidan [23] highlighted the challenges in DC bus voltage control in microgrids, relevant to DC motor control problems in a wider environment. Related research by Jasim and Abd [24] and Aazmi *et al.* [25] highlighted system performance improvement through optimisation and cooling techniques, which served as inspiration for the optimisation approach in our study. The results of this study are also expected to inspire innovation in vehicle control technology as described by Pramudi et al [26] and Wibowo [27], as well as wider applications in energy control systems as presented by Islam et al [28] and Selamat *et al.* [29] and Shamitha *et al.* [30]. The optimisation approach used in our research takes inspiration from the technique used by Nurul Hajar *et al.* [31] in 3D printing parameter optimisation, which shows significant potential in the application of more efficient and effective control technology.

The contribution of this article is in Control optimization with MFSMC controller plays an important role in many aspects, in the field of machine communication [32], batching systems in data processing techniques [33] regulation in energy conversion through turbine blade angle [3].

The rest of this paper is organized as follows: Section II explains the mathematical model of a dc motor. The design of PID controller describes in Section III, while Section IV describes design of MFSMC controller. Section V addresses the simulation results and analysis of result controller, and Section VI provides the conclusions.

2. Methodology

2.1 DC Motor Model

In this paper a schematic diagram of a DC motor is shown in Fig. **1**. The speed control of DC motor is provided by a fixed permanent magnetic field and adjusting armature voltage. The difference between voltage from feeder (e_a) and voltage at the motor terminals (e_b) is calculated using Equation (1), where the R_a is armature resistance (Ω), i_a is armature current (A), L_a is armature inductance (H), and differential of armature current (i_a) versus time (dt). The voltage at the motor terminals ($e_b(t)$) is expressed in Eq. (2), where K_b is electromotive force constant (V.s/rad) and ω is angular speed of motor shaft (rad/s). The ($i_a(t)$) is determined by (3) with K_b is electromotive force constant (V.s/rad). The torque of the load inertia (*T(t)*) is determined using Eq. (4), where the *J* is inertia torque of motor (kg.m^2).T_L is load torque (N.m) and *B* is motor friction constant (N.m.s/rad). The *T(t)* can also be calculated by multiplying the motor torque constant (K_t) and i_a as show in Equation (5). Laplace transform of the ratio of $\omega(s)$ dan e_a(s) for DC motor according to Fig. **1**, simply is shown as Equation (6) and e_b(s) for DC motor is solved with Equation (7), and torque motor is calculated by Equation (8). Correlation motor speed $\omega(s)$ s a function of the armature voltage $e_a(s)$ expression by Equation (9). Equation (10) refines this expression, simplifying it to emphasize the combined effects of these parameters on the motor's behavior.

The Equation (11) further simplifies the motor's speed response, reducing the transfer function to a more concise form, which illustrates the motor's overall response characteristics as influenced by the applied armature voltage. Finally, Equations (12) and (13) offer a state-space representation of the system, where the state variables $\dot{X}_1$and $\dot{X}_2$ represent the motor's angular speed and its derivative.

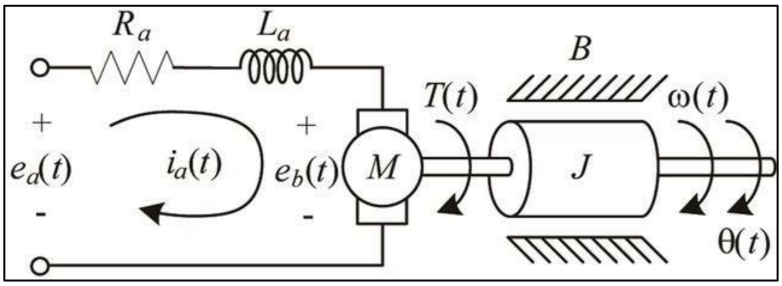

Fig. 1. DC Motor Schematic Diagram

Table 1
DC Motor parameter

Parameter	Value
Armature resistance R_a	0.4 Ω
Armature inductance L_a	2.7 H
Moment of inertia J	0.0004 kg.m2/s2
Fiscous friction B	0.0022 N.m.s/rad
Torque coefficient K_t	0.015 N.m/A
Back emf coefficient K_b	0.05 V.s/rad

$$e_a(t) - e_b(t) = R_a i_a(t) + L_a \frac{di_a(t)}{dt} \tag{1}$$

$$e_b(t) = K_b \omega(t) \tag{2}$$

$$i_a(t) = \frac{e_a(t)}{L_a} - \frac{K_b}{L_a}\omega(t) - \frac{R_a}{L_a} i_a(t) \tag{3}$$

$$T(t) = T_l + J\frac{d\omega(t)}{dt} + B\omega(t) \tag{4}$$

$$T(t) = K_t i_a(t) \tag{5}$$

$$E_a(s) = (L_a s + R_a) I_a(s) + E_b(s) \tag{6}$$

$$E_b(s) = K_b \omega(s) \tag{7}$$

$$T(s) = K_t I_a(s) \tag{8}$$

$$\frac{\omega(s)}{e_a(s)} = \frac{\frac{K_t}{JL_a}}{\left(\left(\left(s + \frac{R_a}{L_a}\right)\left(s + \frac{B}{J}\right)\right) + \frac{K_b K_t}{JL_a}\right)} \tag{9}$$

$$e_a \frac{K_t}{JL_a} = \ddot{\omega} + \left(\frac{R_a}{L_a} + \frac{B}{J}\right)\dot{\omega} + \left(\frac{R_a}{L_a}.\frac{B}{J} + \frac{K_b K_t}{JL_a}\right)\omega \tag{10}$$

$$\ddot{\omega} + 5.64\dot{\omega} + 1.509\omega = 13.89e_a \tag{11}$$

$$X_1 = \omega(t),\ X_2 = \dot{X}_1 = \dot{\omega}(t),\ \dot{X}_2 = \ddot{\omega}(t),\ Y = X_1 = \omega(t),\ u = e_a(t) \tag{12}$$

$$\dot{X}_2 = -5.64X_2 - 1.509X_1 + 13.89u \tag{13}$$

Fig. 2 shows the block diagram of control system with optimizer for DC motor speed control. The analysis of chattering in an optimized model-free sliding mode controller for DC motor speed control follows a structured approach. Initially, the controller is designed without relying on a predefined model, employing optimization to determine the optimal switching gain K and the constant λ slope for the sliding surface. As illustrated, the reference input is combined with feedback from the motor's output to compute an error, which is then sent to both the controller and the optimizer.

The optimizer uses an algorithm guided by the ITAE (Integral of Time-weighted Absolute Error) objective function to process the error and identify the ideal values K and the constant λ slope. These values are then utilized by the controller to regulate the motor, achieving optimal control performance and reducing chattering.

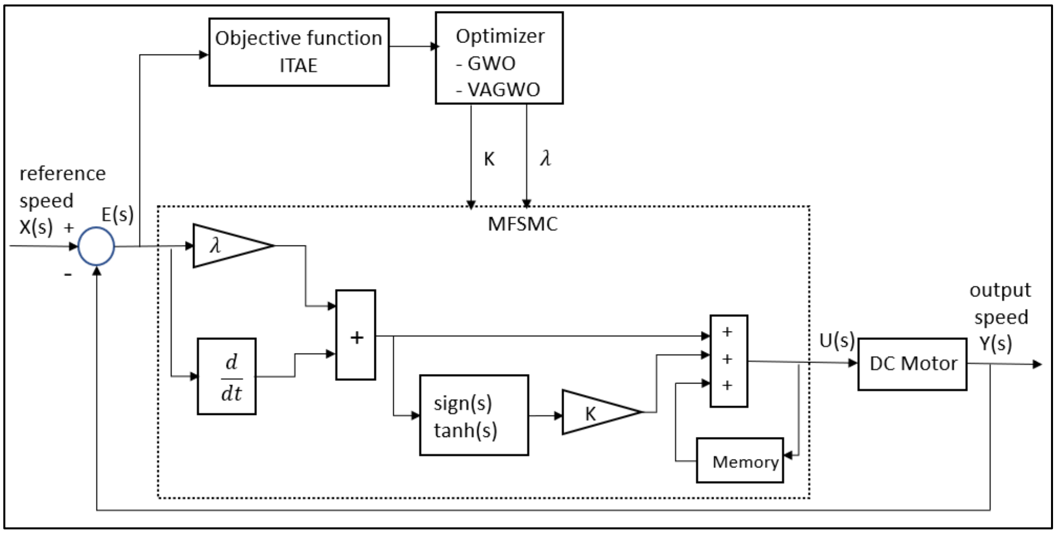

Fig. 2. The block diagram of control system with optimizer for DC motor speed control

2.2 Parameter Setting

Table 5 shows the Parameter settings of the GWO and VAGWO Algorithms used in the model simulation using MATLAB. The simulation results table presents the parameter settings for two algorithms, namely GWO and VAGWO, used in the experiment. The GWO algorithm has a parameter setting of a=[2,0], while VAGWO has several parameter settings, including c=[1,0], a=[√2,0], k=[0.9,0.4], and v_max=0.1[ub-lb]. Both algorithms employ 30 search agents and a maximum iteration number of 50. The lower bounds for k and λ are [0.1 0.1], whereas the upper bounds are [5000 5000]. With these parameters, both algorithms are expected to conduct effective searches and achieve the desired outcomes within the specified number of iterations.

Table 2
Parameter settings of the GWO and VAGWO Algorithms

Algorithm	Parameter settings
GWO	$a = [2, 0]$
VAGWO	$c = [1, 0]$; $a = [\sqrt{2}, 0]$; $k = [0.9, 0.4]$; $v_{max} = 0.1[ub - lb]$
Search agent	30
Maximum iteration number	50
Lower bounds for k and λ	[0.1 0.1]
Upper bounds for k and λ	[5000 5000]

2.3 Input Control Algorithm

To derive the control input equation, the procedure is outlined as follows:

a) The derivation process follows the conventional sliding mode control format but with the system model replaced by its approximation (14), where n is the system order, x(n) is the system state to be controlled, u is the control input, and uk−1 is the previous control input value.

b) The sliding surface is defined as in (15) with λ being the positive constant slope of the sliding surface, and $\tilde{x}$(t) = x(t) – xd(t), where x(t) is the measured state and xd(t) is the desired state to be tracked. The control rule is defined as in (16). Since the system contains uncertainties, a discontinuous term is added to the control rule to bring the system trajectory to the sliding surface. The control rule is then defined as in (17), where η is a small positive constant, and sign(s) is the signum function of the sliding surface s.

c) The Lyapunov Direct Method is used to ensure the system trajectory is asymptotically stable during the reaching phase when the trajectory is not on the sliding surface. A positive definite Lyapunov candidate function is defined as in (19), meeting the criteria to ensure asymptotic stability. By differentiating the Lyapunov candidate function and substituting it into the sliding surface (20), and substituting equation (14) and the control effort from equation (17), we obtain equation (21). The Lyapunov function is always negative definite for positive values of η, thus satisfying the Lyapunov stability criteria and realizing the control effort u as in equation (17).

d) The control effort and switching gain are obtained through the control rule in equation (17), leading to equation (17), where K is the switching gain to be determined and derived to ensure closed-loop stability according to Lyapunov during the reaching phase, becoming equation (23). The sliding condition, according to equation (21), and the derivative of equation (19) are used to find the minimum value of K as in equation (24).

e) Using the definition of the sliding surface, the system form, and the control rule in equation (22), we get equation (25). From the above derivation, it is concluded that the switching gain K must be greater than or equal to η to ensure stability during the reaching phase.

f) The MFSMC control consists of equivalent control corresponding to the sliding phase reaching phase when s(t) = 0 and switching control corresponding to the reaching phase when s(t) $\neq$

0. Furthermore for reducing the chattering on the signum function, the signum switching function replaced by the tanh switching function that relaxation of the gradient of signum function, so that equation (22) become (26).

$$x^{(n)} \approx x^{(n)} + u - u_{k-1} \tag{14}$$

$$s = (d/dt + \lambda)^{n-1}\tilde{x}(t) \tag{15}$$

$$\hat{u}(t) = -(d/dt + \lambda)^{n}\tilde{x} + u_{k-1} \tag{16}$$

$$u = -(d/dt + \lambda)^{n}\tilde{x} + u_{k-1} - \eta * sgn(s) \tag{17}$$

$$sign(s) = \begin{cases} 1, if\ s > 0 \\ 0, if\ s = 0 \\ -1, if\ s < 0 \end{cases} \tag{18}$$

$$V(x) = \frac{1}{2}s^2 > 0 \tag{19}$$

$$\dot{V}(x) = s\left[\left(\frac{d}{dt} + \lambda\right)^{n}\tilde{x}(t)\right] \tag{20}$$

$$\dot{V}(x) = -\eta|s| < 0 \tag{21}$$

$$u = -(d/dt + \lambda)^{n}\tilde{x} + u_{k-1} - K * sgn(s) \tag{22}$$

$$s\dot{s} = \frac{1}{2}\frac{d}{dt}s^2 \leq -\eta|s| \tag{23}$$

$$-K|s| \leq -\eta|s| \tag{24}$$

$$K \geq \eta \tag{25}$$

$$u = -(d/dt + \lambda)n\ \tilde{x} + uk - 1 - K * tanh(s) \tag{26}$$

2.4 Chattering Reduction

Conventional SMC schemes often experience chattering, which is a high-frequency oscillation in the switching control law. A large switching control gain can speed up convergence but causes chattering at steady state, while a small gain causes slow convergence. To avoid high-frequency oscillations in the controlled system, smooth switching is required, which is strongly recommended in the literature. Chattering in the control input can make DC motor applications impractical, so fractional approximation, saturation, or hyperbolic tangen (tanh) functions are used to smooth the control input in SMC schemes with relative degree one or two. In addition, drift, twisting, super-twisting, and sub-optimal sliding mode controllers are developed to overcome chattering without requiring a model of the controlled system. A tanh-based super-twisting controller was also recently proposed to produce smoother control inputs, making the tanh function a top choice in smoothing SMC control inputs. In this study, to achieve smooth transitions in switching control, tanh functions with smoothing constants are used instead of sign functions.

Therefore, in this article, we apply a tanh function with a smoothing constant in place of the sign function to achieve smoother transitions in switching control. This approach is designed to reduce chattering effects and improve system stability, ensuring smoother and more efficient responses. As a result, the method not only optimises control performance but also improves reliability and practical application to various control systems. The implementation of the tanh function in this context offers an innovative solution that can be applied to complex and diverse control scenarios, as outlined as in (14).

a. GWO (*Grey Wolf Optimizer*)

Grey Wolf Optimizer (GWO) was developed by Mirjalili et al. in 2014 [22]. This metaheuristic algorithm uses swarm intelligence to mimic the leadership hierarchy and hunting behavior of grey wolves in nature, translating these behaviors into mathematical models. Grey wolves prefer to live and hunt in packs, and their population is divided into four hierarchical groups: alpha, beta, delta, and omega.

The alpha wolves are the leaders, making all critical decisions regarding hunting. The betas, who occupy the second level, assist the alphas in decision-making and other group activities. The delta wolves follow the alphas and betas but dominate the omegas, who are at the lowest level of the hierarchy and submit to the other wolves. Essentially, if a wolf is neither an alpha nor a beta, it is a delta. The most crucial wolves in the pack are the alphas and betas, as they guide the omegas to regions with the highest hunting potential. This structured approach ensures efficient and strategic hunting, which the GWO algorithm leverages to solve optimization problems effectively.

The Grey Wolf Optimizer (GWO) begins the optimization process by randomly generating a pack of wolves (initial solutions). In each iteration, the three fittest wolves, known as alpha, beta, and delta, are identified as the leaders, while the remaining wolves are called omegas. The omegas encircle the best wolves to explore the most promising regions in the search space. These wolves act as search agents, aiming to find the optimal solution to the optimization problem. As each search agent circles the three best agents in the search space, the arithmetic average of the updated positions of the alpha, beta, and delta wolves is ultimately adopted as the new position for each search agent. This process helps guide the search towards the optimal solution efficiently.

b. VAGWO (Velocity Aided Grey Wolf Optimizer)

In the original Grey Wolf Optimizer (GWO) [34], the search agents lack velocity as a defining feature to aid them in their exploration process. Their movement within the search space relies solely on sequential adjustments of their velocity towards the leading agents, resulting in irregular and discontinuous motion from one iteration to the next. This means that a particular search agent might approach a leading agent in the current iteration, but if the leading agent shifts its position, the search agent promptly alters its trajectory to follow the new lead. Consequently, this fragmented movement pattern among search agents within the search space may lead to potential deviations, causing the loss of numerous potentially beneficial positions within the search space and thus resulting in premature convergence.

Introducing the notion of velocity could serve to address these issues, aiding search agents in maintaining consistent trajectories and enhancing their exploration capabilities. This approach could help strike a balance between exploration and exploitation phases during the optimization process, ultimately averting premature convergence. In the Velocity-Aided Grey Wolf Optimizer (VAGWO), initial random velocities are assigned to each search agent (wolf) when deciding their movements towards the alpha, beta, and delta wolves, and initial random positions are determined for each agent (wolf) within the search space. Consequently, each search agent assumes both velocity and position in each dimension of the optimization problem. Following this, the agents undergo evaluation, and the three most promising agents are designated as the alpha, beta, and delta wolves, tasked with guiding the remaining agents (omega wolves) towards optimal solutions.

3. Results and Discussion

The control model of Fig. 2 has been successfully simulated using MATLAB SIMULINK program by observing the response of the plant system with the implementation of swithing tnah function and swithing sign function in the Grey Wolf Optimizer (GWO) model and Velocity Aided Grey Wolf Optimizer (VAGWO) model. presented as in Fig. 4.

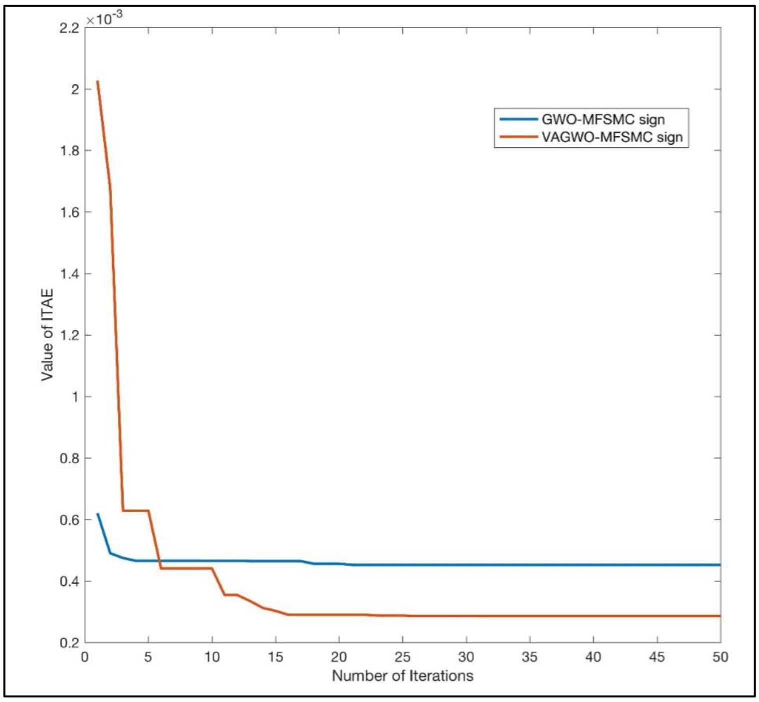

Fig. 3. Optimisation performance of GWO-MFSMC and VAGWO-MFSMC algorithms with ITAE objective function

Simulation is carried out using MATLAB SIMULINK program where GWO and VAGWO optimisers are subjected to sign and tanh switching functions separately. Implements of gain (K) and slope (λ) values are from 0.1 to 5000 to obtain the optimisation parameter values, then these optimisation parameter values are used in the control system. The simulation results show a fast system response to follow the reference signal.

Table 3 shows the Integral of Time-weighted Absolute Error (ITAE) serves as a method to evaluate the control system's performance by assessing the error between the desired output and the actual output. ITAE measures the quality of the control system's response, with a focus on minimizing errors over a longer duration. In the context of a DC motor control system, ITAE is used to gauge the performance of the controller regulating the motor's speed, ensuring prompt attainment of the desired speed while minimizing long-term errors.

Simulation results indicate that the GWO-MFSMC algorithm with the sign switching function yielded an ITAE of 0.00045. Conversely, the VAGWO-MFSMC algorithm with the sign switching function produced a lower ITAE.

The lower ITAE value associated with VAGWO-MFSMC suggests its superiority in minimizing long-term errors compared to GWO-MFSMC. This implies that the VAGWO-MFSMC controller achieves the desired motor speed more rapidly and consistently maintains optimal performance despite disturbances or speed variations.

Thus, these simulation findings affirm that VAGWO-MFSMC with the sign switching function outperforms GWO-MFSMC concerning ITAE, making it the preferable choice for a DC motor control system.

Table 3
ITAE performance optimization

Algorithm-Controller	Switching Function	Performance indices
		ITAE
GWO-MFSMC	sign	0.00045
VAGWO-MFSMC	sign	0.00029

Based on the simulation results presented in Table 4, the control parameters (k and λ) for both algorithms (GWO-MFSMC and VAGWO-MFSMC) demonstrate relative stability, despite variations in the switching functions (sign and tanh). For the GWO-MFSMC algorithm with the sign switching function, the value of k is 5000.00 and λ is 83.16, while for the VAGWO-MFSMC algorithm with the sign switching function, the value of k is 4999.96 and λ is 114.91. When the switching function is changed to tanh, the value of k remains the same for both algorithms (5000.00 for GWO-MFSMC and 4999.96 for VAGWO-MFSMC), while the value of λ changes to 83.16 for GWO-MFSMC and 114.91 for VAGWO-MFSMC. This indicates that the control parameters have been well optimized to achieve the desired performance in the DC motor control system, unaffected by variations in the switching functions. Both algorithms, GWO-MFSMC and VAGWO-MFSMC, demonstrate comparable abilities in producing stable and effective control parameters, whether with the sign or tanh switching functions. The response of the DC motor control system remains consistent and stable despite changes in the switching functions, indicating good adaptability to these variations. Thus, these simulation results confirm that the DC motor control system has exhibited stable and effective performance, with the ability to maintain optimal performance under various control settings.

Table 4
MFSMC controller parameters for DC motors by various algorithms

Algorithm-Controller	Switching Function	Controller Parameter	
		k	λ
GWO-MFSMC	sign	5000.00	83.16
VAGWO-MFSMC	sign	4999.96	114.91
GWO-MFSMC	tanh	5000.00	83.16
VAGWO-MFSMC	tanh	4999.96	114.91

3.1 Tracking Respons Model

Fig. 4 shows the tracking performance of switching functions. In our model analysis realm, the electrifying scene unfolds as the DC motor surges with operational voltage. Amidst this charged atmosphere, the model reveals its intrinsic nature, while the reference response exudes an air of ideal perfection. Enter the GWO-MFSMC sign and VAGWO-MFSMC sign functions, casting hues of blue and yellow across the canvas, painting a vivid portrait of relentless high-frequency ripples that ripple ceaselessly. In this captivating display, the GWO-MFSMC sign and GWO-MFSMC tanh lines move in tandem, while the VAGWO-MFSMC sign line confidently ascends above its tanh counterpart. Rise time, a pivotal measure, steps into the spotlight on our stage. Here, VAGWO tanh shines brightest, boasting a lightning-fast rise time of 0.0269, a compelling testament to its swift responsiveness. Amidst the commotion, both GWO-MFSMC sign and VAGWO-MFSMC sign harmonize softly, their impact subtle yet profound. Nevertheless, amidst this orchestration, GWO-MFSMC tanh and VAGWO-MFSMC tanh take the lead, gracefully converging to meet the reference line with unwavering precision, underscoring the undeniable prowess of the tanh switch function in guiding them towards optimal performance.

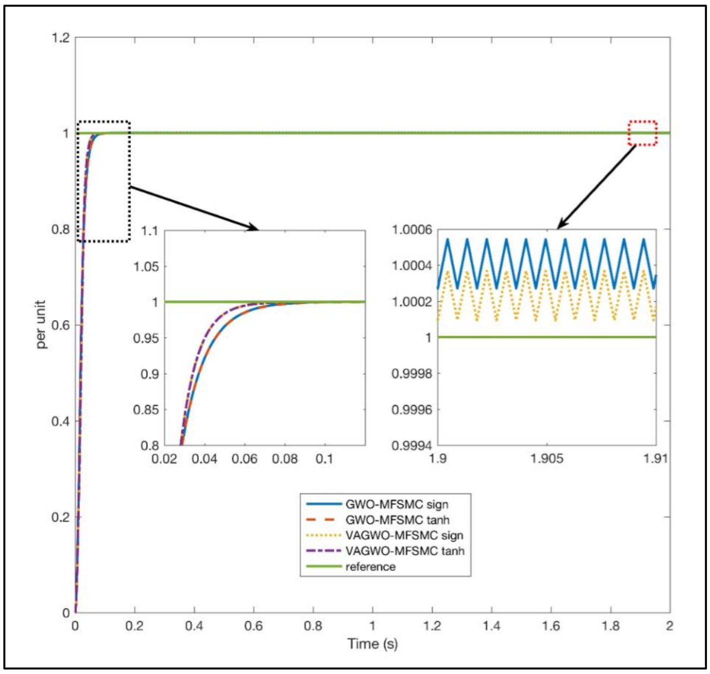

Fig. 4. The tracking performance of switching functions

Table 5 presents the response performance of the GWO-MFSMC and VAGWO-MFSMC algorithms under different switching functions. The table shows that the VAGWO-MFSMC algorithm with the tanh switching function has the smallest rise time, indicating that this algorithm produces the fastest response compared to the other three algorithms.

The smallest settling time value is also achieved by the VAGWO-MFSMC algorithm. This implies that this algorithm facilitates a rapid response to reach the steady state.

Regarding overshoot, both the GWO-MFSMC and VAGWO-MFSMC algorithms with the tanh switching function result in zero overshoot. This indicates that the tanh switching function effectively eliminates overshoot in the system.

Table 5
Profile Response Perfomance

Algorithm-Controller	Switching Function	Response Perfomance		
		Rise time (s)	Settling time (s)	Overshoot (%)
GWO-MFSMC	sign	0.0302	0.0566	0.0089
VAGWO-MFSMC	sign	0.0270	0.0482	0.0088
GWO-MFSMC	tanh	0.0302	0.0565	0
VAGWO-MFSMC	tanh	0.0269	0.0481	0

3.2 Controller Input Result

The importance of the performance of input Controller using GWO-MFSMC and VAGWO-MFSMC controls on the switching sign function lies in its ability to significantly improve the stability and response of the system. GWO-MFSMC and VAGWO-MFSMC. By using this control, it can be observed that the system can quickly adapt to the reference signal.

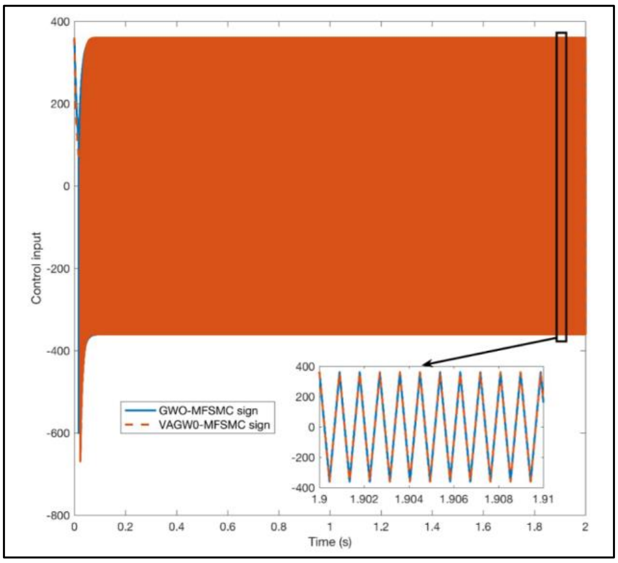

Fig. 5. Chattering Frequency of control input of sign switching function on GWO-MFSMC and VAGWO-MFSMC

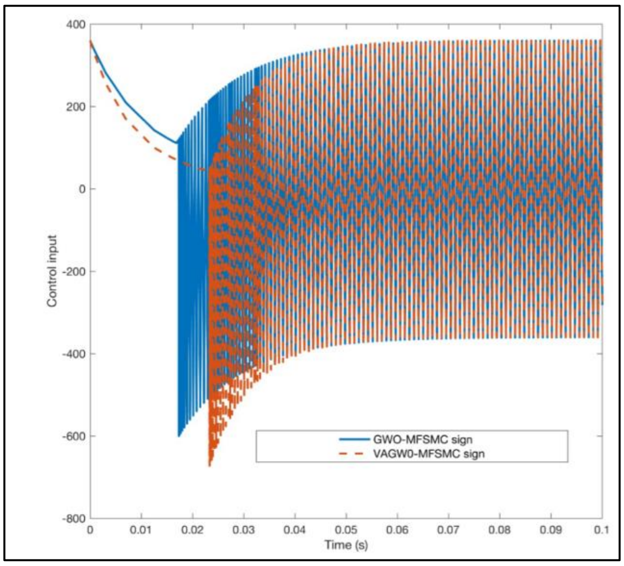

Fig. 6. Control input performance of sign switching function on GWO-MFSMC and VAGWO-MFSMC

Fig. 5 shows the chattering frequency from GWO-MFSMC and VAGWO-MFSMC controls. The results show that GWO and VAGWO with sing switching function produce the same frequency. Control input performance of sign switching function on GWO-MFSMC and VAGWO-MFSMC controls. Control inputs generated from GWO-MFSMC and VAGWO-MFSMC controllers with sign switching function show somewhat different characteristics. GWO-MFSMC and VAGWO-MFSMC produce chattering with a high frequency of 1100 Hz and the same amplitude. Fig. 6 shows the Transient performance from sign switching function on GWO-MFSMC. The GWO-MFSMC sign produces a faster response where the time point of respons on 0.017s. while the response of VAGWO-MFSMC sign occurs at 0.023s.

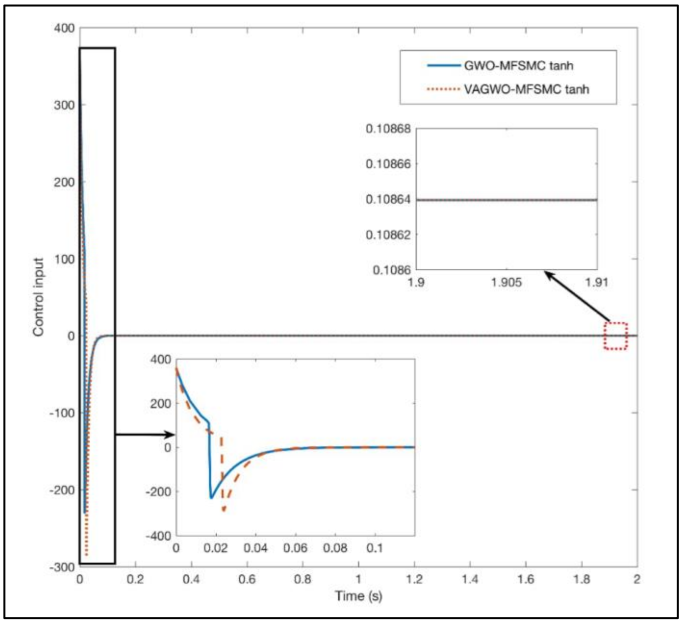

Fig. 7. control input Performance of tanh switching function on GWO-MFSMC and VAGWO-MFSMC controls

Fig. 7 shows the control inputs generated from GWO-MFSMC and VAGWO-MFSMC controllers with tanh transfer function show that the control signals from GWO-MFSMC and VAGWO-MFSMC have no chattering and GWO-MFSMC tanh produces a faster response.

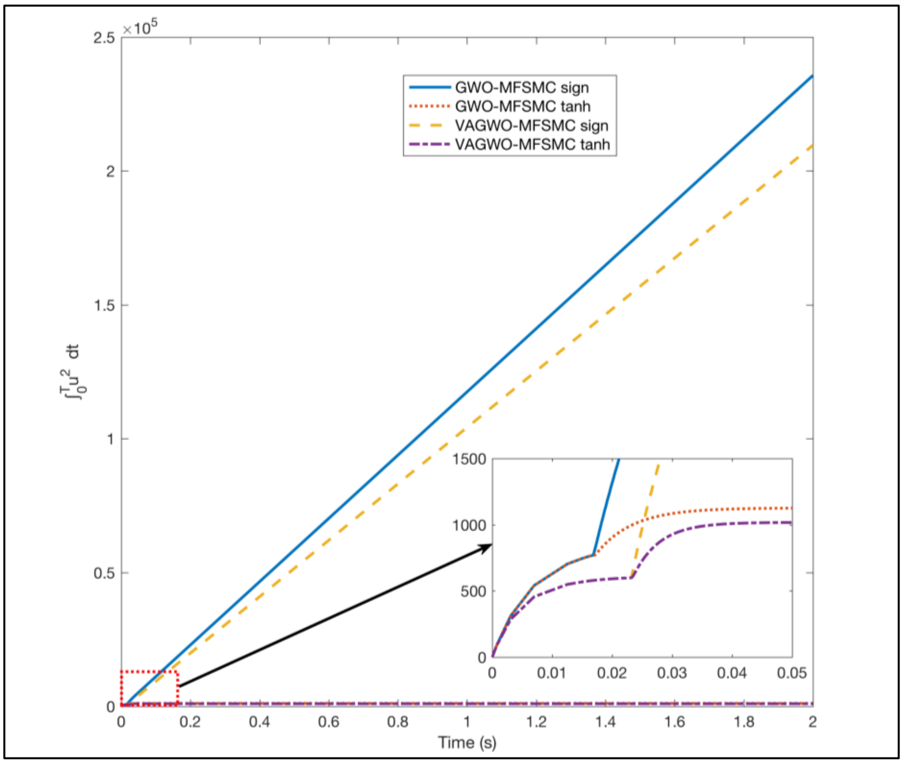

Fig. 8. energy consumption by GWO-MFSMC sign, GWO-MFSMC tanh, VAGWO-MFSMC sign, and VAGWO-MFSMC tanh.

Fig. 8 shows the energy consumption profile with the implementation of the control method using various algorithms, namely GWO-MFSMC sign, GWO-MFSMC tanh, VAGWO-MFSMC sign, and VAGWO-MFSMC tanh. From this figure, it can be seen that the GWO-MFSMC sign and GWO-MFSMC tanh algorithms show high energy consumption and continue to grow linearly. Up to 2 seconds, the energy consumption has not reached steady state. In contrast, the VAGWO-MFSMC sign and VAGWO-MFSMC tanh algorithms show low energy consumption, with steady state reached within 0.04 seconds.

Table 6
Comparison of control energy based on controller variation and switching function

Algorithm-Controller	Switching Function	Control Energy $= \int_0^T \boldsymbol{u^2\, dt}$ (Ws)	Energy (Wh)
GWO-MFSMC	sign	235758.15	65.49
VAGWO-MFSMC	sign	209661.81	58.24
GWO-MFSMC	tanh	1126.71	0.31
VAGWO-MFSMC	tanh	1018.0	0.28

The control energy, or the energy consumption by the controller to control the DC motor, can be seen in Fig. 8 and Table 6. From these results, it is clear that the VAGWO-MFSMC method with the tanh switching function has the lowest energy consumption, while the GWO-MFSMC with the sign switching function has the highest energy consumption.

shows the average electrical energy consumption by control algorithm. It can be seen that GWO-MFSMC sign and VAGWO-MFSMC sign algorithms consume energy continuously up to infinity, while the control method with GWO-MFSMC and VAGWO-MFSMC algorithms together using the tanh switching function, consume relatively small average energy, which is ≥0.31 Wh. And the energy consumption of the VAGWO-MFSMC algorithm with tanh switching function is the smallest.

4. Conclusions

The performance of four control algorithms, GWO-MFSMC and VAGWO-MFSMC, on a DC motor model using sign and tanh switching functions has been successfully observed using MATLAB and SIMULINK. A sliding mode control model, based solely on state measurement and previous control input, has been designed. To reduce the chattering effect, a boundary layer smoothing technique was employed within the controller. This controller, when implemented for speed control of the DC motor, proved to be robust and stable. The sliding condition was maintained at all times and the control effort response was smooth.

Several additional observations can be made: higher values of gain (K) and slope (λ) result in a faster system response. Regarding system response, the VAGWO-MFSMC algorithm significantly impacts rise time and settling time, and the tanh switching function influences the system's overshoot. In terms of energy efficiency, implementing the switching functions in the GWO-MFSMC and VAGWO-MFSMC algorithms has been shown to reduce energy consumption in the DC motor control technique.

Acknowledgement
This article is a dissertation for the Doctoral Program in Engineering at Udayana University, Denpasar, Indonesia. The author extends heartfelt thanks to the Ministry of Education, Culture, Research, and Technology (Kemendikbud-Ristek) and Siliwangi University for their support.

References

[1]. Slotine, Jean-Jacques E. "Applied Nonlinear Control." *PRENTICE-HALL google schola* 2 (1991): 1123-1131.
[2]. Utkin, Vadim, Jürgen Guldner, and Jingxin Shi. *Sliding mode control in electro-mechanical systems*. CRC press, 2017.
[3]. Schulken, Eric, and Agamemnon Crassidis. "Model-free sliding mode control algorithms including application to a real-world quadrotor." In *Pro-ceedings of the 5th International Conference of Control, Dynamic Systems, and Robotics (CDSR'18), Niagara Falls, Canada—June 7–9*. 2018. https://doi.org/10.11159/cdsr18.112
[4]. Crassidis, Agamemnon, and Arielle Mizov. "A model-free control algorithm derived using the sliding mode control method." In *Proceedings of the 2nd International Conference of Control, Dynamic Systems, and Robotics*, pp. 1-9. 2015.
[5]. Crassidis, Agamemnon, and Raul Mittmann Reis. "Model-free sliding mode control method." In *Proceedings of the 3rd International Conference of Control, Dynamic Systems, and Robotics*. 2016. https://doi.org/10.11159/cdsr16.100
[6]. Sreeraj, Adarsh Raj Kadungoth. *A Model-Free Control Algorithm Based on the Sliding Mode Control Method with Applications to Unmanned Aircraft Systems*. Rochester Institute of Technology, 2019.
[7]. Crassidis, Agamemnon, and F. E. Tin. "A Model-Free Control System Based on the Sliding Mode Control Method with Applications to Multi-Input-Multi-Output Systems." In *Proceedings of the 4th International Conference of Control, Dynamic Systems, and Robotics*, no. 119. 2017. https://doi.org/10.11159/cdsr17.119
[8]. Radac, Mircea-Bogdan, Raul-Christian Roman, and Emil M. Petriu. "Model-free sliding mode control of nonlinear systems: Algorithms and experiments." (2017). https://doi.org/10.1016/j.ins.2016.11.026
[9]. Cömert, Ceren, and Coşku Kasnakoğlu. "Comparing and developing PID and sliding mode controllers for quadrotor." *International Journal of Mechanical Engineering and Robotics Research* 6, no. 3 (2017): 194-199. https://doi.org/10.18178/ijmerr.6.3.194-199
[10]. Vrkalovic, Sasa, Elena-Cristina Lunca, and Ioan-Daniel Borlea. "Model-free sliding mode and fuzzy controllers for reverse osmosis desalination plants." *Int. J. Artif. Intell* 16, no. 2 (2018): 208-222.
[11]. Khooban, Mohammad-Hassan. "Secondary load frequency control of time-delay stand-alone microgrids with electric vehicles." *IEEE Transactions on Industrial Electronics* 65, no. 9 (2017): 7416-7422. https://doi.org/10.1109/TIE.2017.2784385
[12]. Gao, Peng, Xiaodong Lv, Huimin Ouyang, Lei Mei, and Guangming Zhang. "A Novel Model-Free Intelligent Proportional-Integral Supertwisting Nonlinear Fractional-Order Sliding Mode Control of PMSM Speed Regulation System." *Complexity* 2020, no. 1 (2020): 8405453. https://doi.org/10.1155/2020/8405453
[13]. Lin, Chien-Hong, and Fu-Yuen Hsiao. "Proportional-integral sliding mode control with an application in the balance control of a two-wheel vehicle system." *Applied Sciences* 10, no. 15 (2020): 5087. https://doi.org/10.3390/app10155087
[14]. Ebrahimi, Nahid, Sadjaad Ozgoli, and Amin Ramezani. "Model free sliding mode controller for blood glucose control: Towards artificial pancreas without need to mathematical model of the system." *Computer Methods and Programs in Biomedicine* 195 (2020): 105663. https://doi.org/10.1016/j.cmpb.2020.105663
[15]. Chen, Xiangjian, Di Li, Pingxin Wang, Xibei Yang, and Hongmei Li. "[Retracted] Model-Free Adaptive Sliding Mode Robust Control with Neural Network Estimator for the Multi-Degree-of-Freedom Robotic Exoskeleton." *Complexity* 2020, no. 1 (2020): 8327456. https://doi.org/10.1155/2020/8327456
[16]. Moya-Lasheras, Eduardo, Edgar Ramirez-Laboreo, and Carlos Sagues. "Model-free sliding-mode controller for soft landing of reluctance actuators." *IFAC-PapersOnLine* 53, no. 2 (2020): 6256-6261. https://doi.org/10.1016/j.ifacol.2020.12.1738
[17]. Ghalimath, Prabhudev, and S. S. Sankeswari. "Speed control of DC motor using sliding mode control approach." *IOSR J. Electr. Electron. Eng* 10, no. 4 (2015): 17-22. DOI: 10.9790/1676-10411722
[18]. Dursun, Emre Hasan, and Akif Durdu. "Speed control of a DC motor with variable load using sliding mode control." *International Journal of Computer and Electrical Engineering* 8, no. 3 (2016): 219. https://doi.org/10.17706/IJCEE.2016.8.3.219-226
[19]. Moussavi, S. Z., M. Alasvandi, and Sh Javadi. "Speed control of permanent magnet DC motor by using combination of adaptive controller and fuzzy controller." *International Journal of Computer Applications* 52, no. 20 (2012). https://doi.org/10.5120/8316-1774
[20]. Hiron, Nurul, and Asep Andang. "Wireless communication with batching method based on Xbee-PRO S2B module for sensing of wind speed." In *2016 2nd International Conference on Science in Information Technology (ICSITech)*, pp. 250-253. IEEE, 2016. https://doi.org/10.1109/ICSITech.2016.7852642
[21]. Busaeri, Nundang, Nurul Hiron, Ida Ayu Dwi Giriantari, Wayan Gede Ariastina, and Ida Bagus Alit Swamardika. "Green Campus Establishment Through Carbon Emission and Energy Efficiency Control." In 2021 International

Conference on Smart-Green Technology in Electrical and Information Systems (ICSGTEIS), pp. 106-111. IEEE, 2021. https://doi.org/10.1109/ICSGTEIS53426.2021.9650356

[22]. Azeem, Fawad, and Hasan A. Zidan. 2024. “DC Bus Voltage Control of Islanded Microgrid Using Renewable Energy Based Distributed Generation.” Journal of Advanced Research in Applied Mechanics 118 (1): 183–92. https://doi.org/10.37934/aram.118.1.183192

[23]. Firdaus, Fahri, Edvin Priatna, Nurul Hiron, and Nundang Busaeri. "Prototype Sistem Kendali Kecepatan Motor Dc Dengan Proportional Integral Derivative (PID) Controller." Journal of Energy and Electrical Engineering 4, no. 1 (2022).

[24]. Jasim, Qusay, and Najim Abd. "Experimental and Theoretical Study to Improve the Performance of Solar Cells by Evaporative Cooling in Iraq." Journal of Advanced Research in Applied Mechanics 100, no. 1 (2022): 1-12. https://doi.org/10.37934/aram.101.1.118.

[25]. Muhamad Akmal Aazmi, Shamshul Bahar Yaakob, Muhammad Izuan Fahmi Romli, and Muhammad Zaid Aihsan. 2024. “Improvement of Based Sector and Comparison Speed and Electromagnetic Torque of Direct Torque Control.” Journal of Advanced Research in Applied Mechanics 120 (1): 158–70. https://doi.org/10.37934/aram.120.1.158170.

[26]. Nurul Hajar, Nurul ‘Aini, Norrlaili Shapiee, Mohd Rivaie, Adam Samsudin, Nor Hafizah Hussin, and Siti Haryanti Hairol Anuar. 2024. “The Application of Conjugate Gradient Methods to Optimize 3D Printed Parameters.” Journal of Advanced Research in Applied Mechanics 120 (1): 136–41. https://doi.org/10.37934/aram.120.1.136141.

[27]. Pramudi, Setia Hadi, Dzikri Putra Abdillah, Helmi Wibowo, and I. Made Suartika. "Prototype Of Inspection Exhaust Brake Vehicle Based Microcontroller." Journal of Energy and Electrical Engineering 5, no. 1 (2023).

[28]. Prof Dr M. Shahidul Islam, Mr Michael Anggie Boniface, Assoc. Prof Dr Rubiyah bt Hj Baini, Dr Ahmad Adzlan Fadzli Bin Khairi, and Mr Hishammudin Afifi bin Huspi. 2024. “Impact of Process Control Devices on the Performance of Ultrafilter Membrane in Clean Water Production.” Journal of Advanced Research in Applied Mechanics 120 (1): 142–57. https://doi.org/10.37934/aram.120.1.142157.

[29]. Selamat, Hazlina, Mohamad Fadzli Haniff, Aminudin Abu, Mohd Azlan Abu, Radhir Sham Mohamad, and Muhammad Nur Azam Azizuddin. 2023. “Development of Web-Based IoT Comfort Index and Electricity Consumption Estimation Monitoring Microcontroller System with Wireless Sensor Modules for Air-Conditioning System.” Journal of Advanced Research in Applied Mechanics 104 (1): 12–24. https://doi.org/10.37934/aram.104.1.1224.

[30]. Shamitha, Asha Crasta, Khizar Ahmed Pathan, and Sher Afghan Khan. 2023. “Numerical Simulation of Surface Pressure of a Wedge at Supersonic Mach Numbers and Application of Design of Experiments.” Journal of Advanced Research in Applied Mechanics 101 (1): 1–18. https://doi.org/10.37934/aram.101.1.118.

[31]. Wibowo, Helmi. "Microcontroller-Based Vehicle Testing Units: Alternative Speed Measurement Tools In Speedometer Testing." *Journal of Energy and Electrical Engineering* 5, no. 2 (2024).

[32]. Mirjalili, Seyedali, Seyed Mohammad Mirjalili, and Andrew Lewis. "Grey wolf optimizer." *Advances in engineering software* 69 (2014): 46-61. https://doi.org/10.1016/j.advengsoft.2013.12.007

[33]. Rezaei, Farshad, Hamid Reza Safavi, Mohamed Abd Elaziz, Shaker H. Ali El-Sappagh, Mohammed Azmi Al-Betar, and Tamer Abuhmed. "An enhanced grey wolf optimizer with a velocity-aided global search mechanism." *mathematics* 10, no. 3 (2022): 351. https://doi.org/10.3390/math10030351